Hunt, G. W., Lord, G. J., & Champneys, A. R. (1998). Homoclinic and heteroclinic orbits underlying the post-buckling of axially-compressed cylindrical shells.

Early version, also known as pre-print

1 Introduction

Buckling of elastic structures at symmetric bifurcation points is broadly classifiable as either supercritical or subcritical, depending on whether the bifurcation point itself is stable or unstable (Koiter 1945, Thompson & Hunt 1973). For a structure that is long in comparison with the wavelength of the buckle pattern, quite different forms of behaviour would be expected to emanate from each. A supercritical bifurcation typically leads to a post-buckling response that is periodic along the length, but subcritical responses are likely to localize, such that the buckle pattern is spread effectively only over a small range of a spatial length variable x. For such responses, provided the structure is sufficiently long and buckling does not occur close to the boundaries, x may be regarded locally as ranging over an infinite 'time-like' domain. Hence, employing a dynamical systems analogy, as in (Hunt, Bolt & Thompson 1989), a localised response represents a so-called *homoclinic connection*, from the unbuckled (fundamental) equilibrium state to itself. Near a subcritical bifurcation spatially periodic responses may also exist, but they require more energy to trigger and hence will not appear in a physical test. Analytically and numerically however, periodic solutions abound, and as a result they often mask the appearance of the localization.

There is a developing body of literature on localization problems in elastic systems, with several recent extensions into related viscous and visco-elastic behaviour (see for example Tvergaard & Needleman (1980) and Potier-Ferry (1983) for early work and Champneys, Hunt & Thompson (1997) for a recent collection). In fact, the situation is often yet more complicated because, in dynamical systems terms, the structural bifurcation point represents a subcritical Hamiltonian-Hopf bifurcation and it is known that such a bifurcation gives rise to infinitely many additional complex paths of 'multi-humped' localised responses (see, e.g. (Buffoni, Champneys & Toland 1996, Iooss & Peroueme 1993) and Section 4 below for more details). Largely these extra localised modes are not important, and it is the primary (or ground state) mode that is physically stable under appropriate loading conditions. However, as we see in Section 4, certain of these multi-humped states do play a role in the mechanism we wish to uncover.

Specifically we are thinking of the following situation. If a system has the potential first to destabilize and then restabilize, such that the underlying potential energy function at the critical bifurcation point has the form of a local maximum within a global minimum, both localization and periodicity can appear in the same topology. Under parametric change in load the possibility then exists of a connection between the fundamental equilibrium state and a periodically buckled equilibrium state (see Fig. 2 below). In dynamical terms this is a *heteroclinic connection* between one equilibrium state and another. An earlier asymptotic approach (Hunt & Lucena Neto 1993) links the phenomenon to the classical *Maxwell load* of the periodic response, but to our knowledge, examination in the full spatial context has up to now been lacking. There is however a broad class of problems to which it should apply, including the example worked out in detail here – the axially-compressed cylindrical shell. For such systems, a mechanism for explaining the postbuckling behaviour is fundamentally important since the effective (observed) buckling load may be much smaller than the bifurcation (predicted) load. In the case of the cylinder the effective buckling load may be as little as a quarter of the bifurcation load.

After presenting in Section 2 a succinct derivation of energetic and equilibrium equations for a cylindrical shell, we provide an explanation of the homoclinic/heteroclinic mechanism

on three different levels. First, in Section 3, we review a multiple scale asymptotic portrayal, the so called 'slow-space' description, in which the heteroclinic connection appears at a single distinct load. Next, in Section 4, by using a generic dynamical systems unfolding of the assumed global bifurcation sequence, it is demonstrated that heteroclinic connections will, in fact, range over a sequence of loads. Moreover, the bifurcation sequence from the homoclinic to the heteroclinic response causes a succession of 'compartmentalized' buckles via an infinite sequence of snaking destabilizing and restabilizing folds. Finally, in Section 5, the preceding theory is confirmed by numerical continuation analysis of a discretization the equilibrium equations of the cylinder. Section 6 draws conclusions. We find that the slow space portrayal allied with its dynamical systems interpretation is remarkably successful, predicting not only appearance of the heteroclinic connection itself, but also its close relationship with the practically-important first minimum load encountered on the post-buckling equilibrium path. The asymptotics show, in effect, that this minimum load can be interpreted as the classical critical Maxwell load of the periodic potential energy function.

2 Formulation: von Kármán–Donnell Equations and Total Potential Energy

The classical *equilibrium-equation* formulation for a thin (shallow) cylindrical shell of radius R and thickness t usually starts with governing nonlinear von Kármán–Donnell differential equations:

$$\begin{aligned} \kappa^2\nabla^4 w + \lambda w_{xx} - \rho\phi_{xx} &= w_{xx}\phi_{yy} + w_{yy}\phi_{xx} - 2w_{xy}\phi_{xy} \qquad (1)\\ \nabla^4\phi + \rho w_{xx} &= (w_{xy})^2 - w_{xx}w_{yy}, \qquad (2) \end{aligned}$$

where ∇^4 is the two dimensional bi–harmonic operator, $x \in \mathbb{R}$ is the axial and $y \in [0, 2\pi R)$ is the circumferential co-ordinate, w is the radial displacement measured from a non-trivial (fundamental) unbuckled state, and ϕ is a stress function (Koiter 1945). Equations (1) and (2) are supplemented by suitable boundary conditions (eg. for a solution that localizes in x, w, ϕ and their x derivatives may tend to zero, while natural periodic conditions can be assumed in y). Parameters appearing are the curvature $\rho = 1/R$, the geometric constant,

$$\kappa^2 = t^2/12(1-\nu^2),$$

where ν is Poisson's ratio, and the bifurcation parameter,

$$\lambda = P/Et,$$

where P is the compressive axial load applied per unit length and E is Young's modulus. Here (1) is an equilibrium and (2) a compatibility equation.

Alternatively, a *variational* formulation of the problem is obtained upon writing a total potential energy functional $\mathcal{V}$, comprising bending energy,

$$U_B = \frac{Et^3}{24\,(1-\nu^2)} \int_0^L \int_0^{2\pi R} \left\{ \left(\nabla^2 w\right)^2 - 2\,(1-\nu)\left[w_{xx}w_{yy} - (w_{xy})^2\right] \right\} \mathrm{d}x\mathrm{d}y, \qquad (3)$$

the membrane (stretching) energy,

$$U_M = \frac{Et}{2}\int_0^L \int_0^{2\pi R} \left\{ \left(\nabla^2\phi\right)^2 - 2\left(1+\nu\right)\left[\phi_{xx}\phi_{yy} - \left(\phi_{xy}\right)^2\right] \right\} \mathrm{d}x\mathrm{d}y, \tag{4}$$

and the first-order work done by the axial compressive load λ,

$$W = -\frac{Et\lambda}{2}\int_0^L \int_0^{2\pi R} \left(w_x\right)^2 \mathrm{d}x\mathrm{d}y. \tag{5}$$

As they take no account of the constraint of compatibility, these functionals cannot be used directly to find minimum energy configurations. However, a Lagrange multiplier introduced on the compatibility equation (2) gives the usable form:

$$\begin{aligned} \mathcal{V} &= \frac{Et^3}{24\left(1-\nu^2\right)}\int_0^L \int_0^{2\pi R} \left\{ \left(\nabla^2 w\right)^2 - 2\left(1-\nu\right)\left[w_{xx}w_{yy} - \left(w_{xy}\right)^2\right] \right\} \mathrm{d}x\mathrm{d}y \\ &+ \frac{Et}{2}\int_0^L \int_0^{2\pi R} \left\{ \left(\nabla^2\phi\right)^2 - 2\left(1+\nu\right)\left[\phi_{xx}\phi_{yy} - \left(\phi_{xy}\right)^2\right] \right\} \mathrm{d}x\mathrm{d}y \\ &- \frac{Et\lambda}{2}\int_0^L \int_0^{2\pi R} \left(w_x\right)^2 \mathrm{d}x\mathrm{d}y \\ &- Et\int_0^L \int_0^{2\pi R} \phi\left[\nabla^4\phi + \rho w_{xx} - \left(w_{xy}\right)^2 + w_{xx}w_{yy}\right] \mathrm{d}x\mathrm{d}y. \end{aligned} \tag{6}$$

Minimization with respect to w then gives the equilibrium equation (1) and with respect to ϕ the compatibility equation (2).

Since we are not considering finite-length or boundary effects, much of what follows leans heavily on regarding a spatial variable (for the cylinder, the axial co-ordinate x) as time-like and then using energy properties found in the formalizations of Lagrangian and Hamiltonian dynamical systems (see (Mielke 1991) for some general theorems in this direction).

3 Asymptotic Representation

The equilibrium behaviour of a typical one degree-of-freedom (1 d.o.f.) conservative structural system with a fundamental path which loses stability at a subcritical bifurcation point is shown schematically in Fig. 1. If $V(A,P)$ represents the total potential energy, where A measures the degree of freedom and P the load, equilibrium at different but constant values of P is given by $\partial V/\partial A = 0$. The shape of the V-surface then is as shown in Fig. 1, sketched for three typical P-values below, at, and above the critical bifurcation load P^C. For $P < P^C$ we find a surface with a minimum of V flanked by two maxima, evolving under increasing load to one with just a single maximum (Thompson & Hunt 1973).

This single d.o.f. picture can be applied to a long structure that buckles periodically, using Rayleigh-Ritz or some other spectral decomposition combined with Liapunov-Schmidt reduction, see e.g (Golubitsky & Schaeffer 1985). The assumption of periodic fluctuation in space effectively removes any spatial co-ordinates from consideration, giving again simply $V = V(A,P)$ for the energy, where A is now the amplitude of the major harmonic component. Localization or other modulation of the buckle pattern demands reintroduction of spatial variables, and this can be done either by reverting to the full von Kármán–Donnell

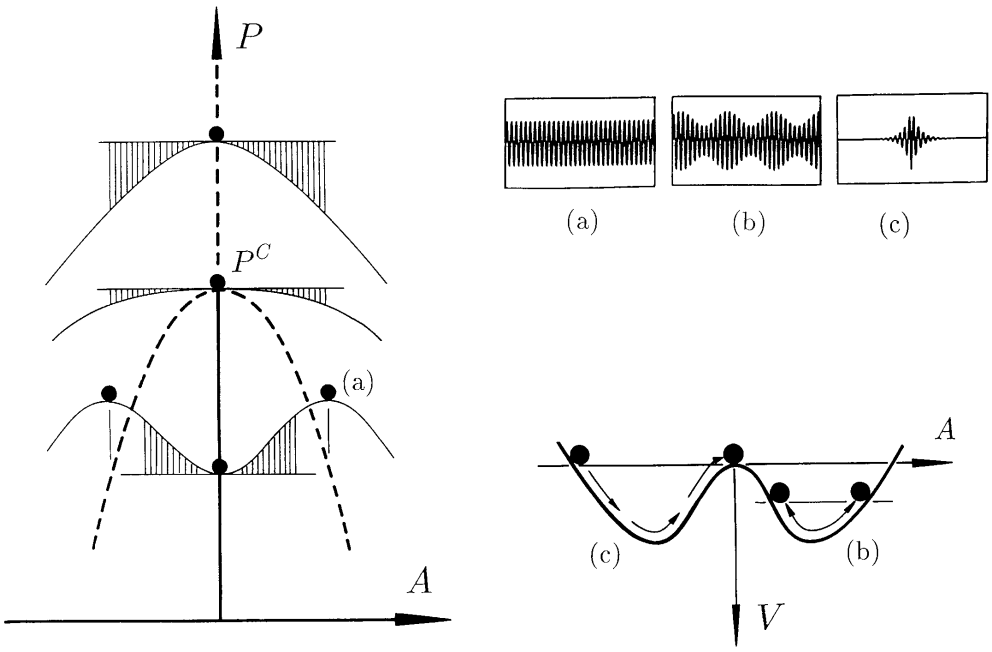

Figure 1: Left: typical subcritical 1 d.o.f. response. Right: asymptotic portrayal in slow space: a) periodic; b) modulated; c) localized.

equations, or in a useful asymptotic sense by assuming that A is slowly varying in space. This view is strictly only valid close to the critical point where $P = P^C$, and it remains one of the central aims of this paper to explore the extent of its validity by comparing predictions with numerical solutions to the full equations.

3.1 Localization – Bifurcation of a Homoclinic Connection

The spatial variable can be reintroduced in an asymptotic sense by writing $X = xs$, where s is a perturbation parameter measuring movement away from the critical point (e.g. $s = (P^C - P)^\alpha$ for some α). As a canonical example, consider the dimensionless model of a compressed strut on a destabilizing quadratic (Winkler) foundation, described by the fourth-order ordinary differential equation for lateral displacement w in terms of axial coordinate x (Hunt et al. 1989, Hunt & Wadee 1991)

$$\ddot{w}\ddot{w} + p\ddot{w} + w - w^2 = 0, \tag{7}$$

where p represents the loading parameter with a critical value of $p = 2$. Dots denote differentiation with respect to 'fast' space x. Taking the ansatz $w(x) = A(X)\cos x$ with $X = x\sqrt{(2-p)}$, then, to lowest order, (7) reduces to the second-order differential equation in A,

$$4A'' - A + \frac{19}{18}A^3 = 0, \tag{8}$$

the prime denoting differentiation with respect to 'slow' space X (Potier-Ferry 1983, Hunt et al. 1989). Note that (8) has the exact pair of homoclinic solutions

$$A(X) = \pm\sqrt{36/19}\,\mathrm{sech}(X/2). \tag{9}$$

However, it is more instructive for the present arguments to view the equation energetically.

In a Lagrangian interpretation of equation (8), spatial potential energy V, expressed by

$$V = \frac{1}{2}A^2 - \frac{19}{72}A^4, \tag{10}$$

is independent of the 'time' measure X; V thus turns out to be the same as the 1 d.o.f. V for a periodic fluctuation of the same system. The 'velocity' dependent or kinetic component of the energy,

$$T = -2(A')^2, \tag{11}$$

involves the first derivative A'. As T is negative definite, the system responds like a ball rolling with conserved total energy $\mathcal{H} = T + V$ in the upside-down version of V, as seen on the right of Fig. 1. For a fully localized solution, the level of V where A is a maximum and hence $A' = T = 0$, must thus match that of the fundamental (unbuckled) path.

3.2 Cylindrical Shell Formulation

Both periodic and localized behaviour of axially-compressed cylindrical shells are known to involve more than just one d.o.f. The nearest equivalent set of equations to (8) for the cylinder problem appears to comprise the three linked nonlinear equations,

$$\begin{aligned} 8(1-\beta^2)^2\kappa^2 A'' - 2A + 3\rho\beta^2 BC &= 0 \\ 16(1+\beta^2)^2\kappa^2 B'' - 4(1+\beta^2)^2 B + 3\rho\beta^2 AC &= 0 \\ 8(1-\beta^2)^2\kappa^2 C'' - 2\beta^4 C + 3\rho\beta^2 AB &= 0 \end{aligned} \tag{12}$$

which were obtained in (Hunt & Lucena Neto 1991) by taking leading-order terms based on the assumed form for w and ϕ,

$$\begin{aligned} w &= A(X)\cos(\gamma x\cos\beta\gamma y) + B(X)\cos((1+\beta^2)\gamma x) + C(X)\cos(\beta^2\gamma x)\cos(\beta\gamma y)\,; \\ \phi &= \kappa A(X)\cos(\gamma x\cos\beta\gamma y) + \kappa B(X)\cos((1+\beta^2)\gamma x) + \kappa C(X)\cos(\beta^2\gamma x)\cos(\beta\gamma y)\,. \end{aligned} \tag{13}$$

The form of (13) is obtained by taking the three interacting modes on the classical *Koiter circle* (Koiter 1945) which describes the neutral stability curve in (γ, β)-space where γ is an axial wavenumber and β an aspect ratio of axial to circumferential wavelength. Corresponding V and T functions are,

$$\begin{aligned} V &= A^2 + 2(1+\beta^2)^2 B^2 + \beta^4 C^2 - 3\rho\beta^2 ABC, \\ T &= -4\kappa^2[(1-\beta^2)^2 A'^2 + 2(1+\beta^2)^2 B'^2 + (1-\beta^2)^2 C'^2], \end{aligned} \tag{14}$$

Again with $T = 0$, V is identical to the integrated total structural potential energy obtained from spectral decomposition combined with Liapunov-Schmidt reduction to the three active degrees of freedom.

In (Hunt & Lucena Neto 1991) it was shown by numerical shooting that the system (12) possess a homoclinic solution that is similar in character (i.e. being symmetric, positive and monotonic up to its point of symmetry) to the positive solution (9) of (8).

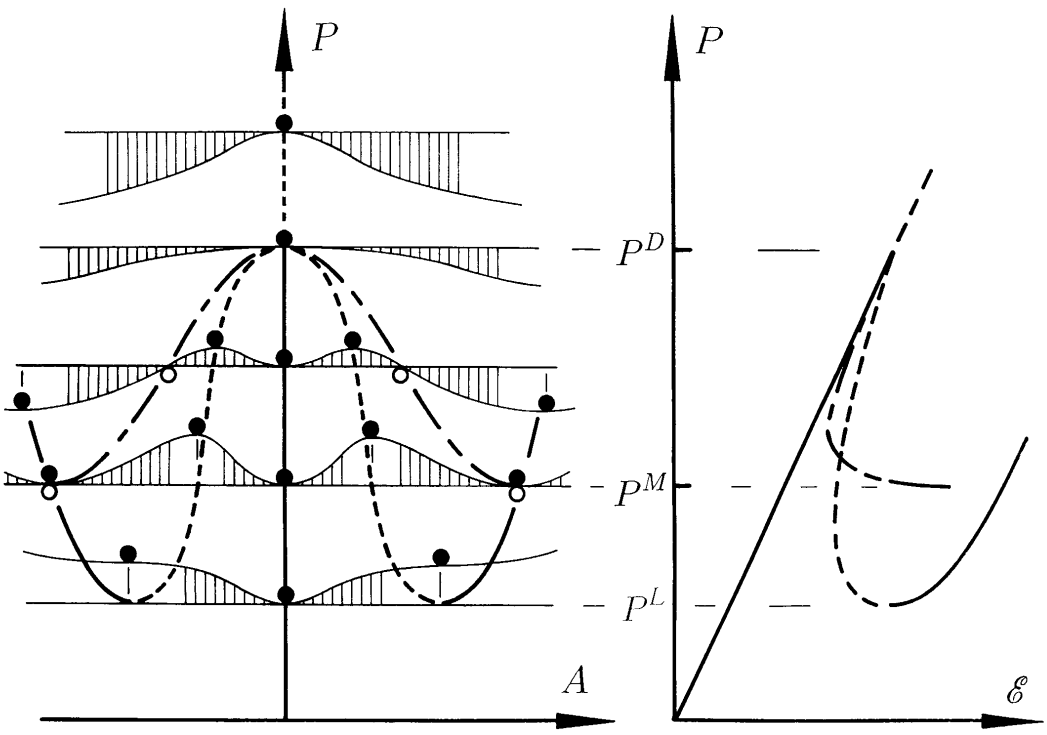

Figure 2: Asymptotic view of Fig. 1, extended to restabilization. $\mathcal{E}$: corresponding deflection of load P. P^D: critical eigenvalue load. P^M: Maxwell load. P^L: minimum post-buckling load for periodic responses.

3.3 Maxwell Load Hypothesis – Heteroclinic Connection

If the slow space concept of Fig. 1 is extended to a system that first destabilizes and then restabilizes, as shown in Fig. 2, several interesting features emerge. Here periodic states for which $\partial V/\partial A = 0$ are shown as black circles, while maximum amplitudes of the localized (homoclinic) solutions, where $A' = T = 0$, are shown as open circles. We see that the minimum post-buckling load for the localized solution must always appear above that for the periodic solution. Moreover at the minimum localized post-buckling load, the two solutions must be one and the same; the periodic state is exactly that which matches the V level of the fundamental path, $A = 0$. Interestingly, this coincides with the classical Maxwell critical load, relevant for stochastic systems governed by basic underlying disturbances or excitations, where the state of stable equilibrium is associated only with the global minimum of V, rather than local minima (see for example Zeeman (1977), pp 306–310); according to the Maxwell convention, states on the fundamental path between P^M and P^D are unstable.

Although having three rather than one essential d.o.f. in its slow-space formulation, it is interesting to extend these ideas to the cylinder problem. Hunt & Lucena Neto (1993) compare Maxwell critical loads obtained from multi-dimensional Rayleigh-Ritz models which are periodic both circumferentially and axially, with experimental results due to Yamaki (1984). It was found that, not only do the Maxwell loads thus obtained match the observed minimum post-buckling loads with surprising accuracy, but so too do the axial

wavelengths of the buckle pattern, which in the Rayleigh-Ritz formulation are allowed to choose themselves by direct energy minimization.

As, over the large deflections involved, the system might well have diverged significantly from the slow-space asymptotic portrayal, these results are sensibly viewed with suspicion. The dynamical view of the following section, for example, demonstrates that the Maxwell criterion must operate over a range of loads, rather than the single load of Fig. 2. It is also debatable whether the cylinder of Yamaki (1984) is long enough for the structural boundary conditions to be clear of influence. Nevertheless, we now have good agreement between numerics and experiments (Lord, Champneys & Hunt (1997, 1998)), and it remains a useful exercise to extend the numerics to capture periodic solutions of any wavelength. This gives a second check on the Maxwell criterion and related predictions, which can be operated entirely independently of all experimental issues.

The numerics, presented Section 5 below, thus provide stronger evidence for both the existence of heteroclinic connections and for their role in linking the Maxwell critical load for periodic solutions with the minimum post-buckling load for localized behaviour. First we apply dynamical systems arguments to put our tentative statements about heteroclinic connections, based on a 1 d.o.f. analogy, on a more sound footing.

4 Dynamical Systems Analogy

We consider an extension to arbitrary d.o.f. Hamiltonian reversible dynamical systems of the concept of the heteroclinic connection in the 1 d.o.f. analogy embodied in Figs. 1 and 2. Here *reversibility* defines the existence of a linear transformation R that fixes half the phase space variables (the co-ordinate variables of a classical Hamiltonian system) and negates the others (the momentum variables), such that the system is invariant under R and a reversal of time (Devaney 1976). Most structural systems have this notion of reversibility; see Section 5 for the reversibilities of the von Kármán–Donnell equations.

Recall, by analogy with the strut model (7) which is equivalent to a 2 d.o.f. Hamiltonian system, that the structural bifurcation at $P = P^C$ corresponds to a *Hamiltonian Hopf* bifurcation (van der Meer 1985) of the trivial equilibrium $w = 0$. At such a point, structural instability occurs when the linearization about the trivial equilibrium involves a complex quadruple of eigenvalues $\pm\mu \pm i\omega$ (a saddle focus) becoming pure imaginary (a centre) as $\mu \to 0$. Under the conditions of subcriticality, then it is known that a pair of reversible homoclinic orbits bifurcate into the region where the equilibrium is a saddle-focus. For the strut model, (7), these two solutions are those expressed asymptotically as (9). In general they represent two sine waves 180° out of phase modulated by a sech-like profile. One of these solutions is identified as being the primary localised mode of buckling as the parameter P moves one away from the critical load. In fact, under generic *transversality* hypotheses, given a primary homoclinic orbit to a saddle-focus, there will be an infinite number of *N-pulse* homoclinic orbits which are like multiple copies of these primaries separated by a finite number of oscillations; see (Champneys 1998) for a review. Note that none of these more complex localised buckling modes will bifurcate from the trivial solution, but instead will remain of finite amplitude and form folds with respect to P for $P < P^C$. In general these solutions are not of interest because they are unlikely to be physically stable (Sandstede 1997) and would require greater triggering energy than the primary localised mode.

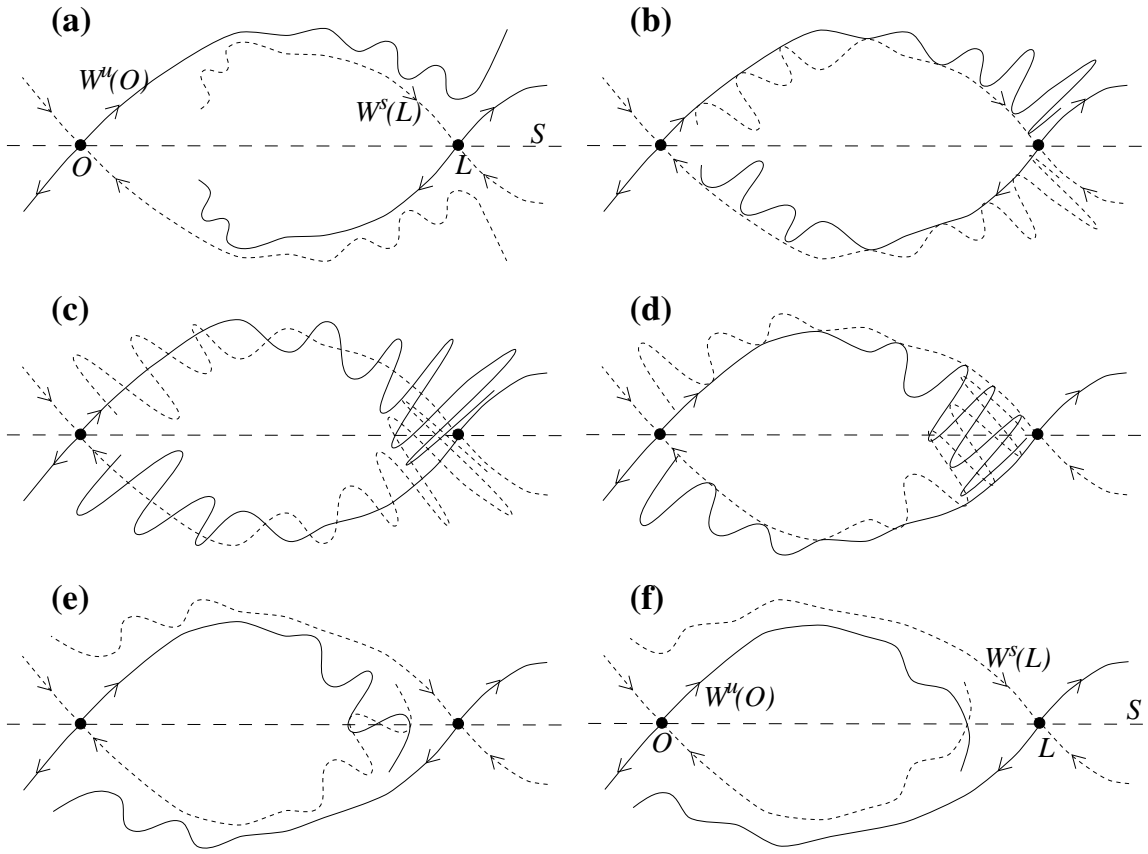

Figure 3: Illustrating the parameter unfolding of two successive heteroclinic tangencies between a saddle-focus equilibrium O and a saddle-type periodic orbit L for a four-dimensional reversible Hamiltonian system. The picture is drawn schematically by taking a formal Poincaré section within the zero level set of the Hamiltonian function (see text for details). Here S is the symmetric section, i.e. fixed point set of the reversibility, and unstable and stable manifolds are depicted respectively by solid and broken lines.

We now suppose that at some other parameter value the primary homoclinic orbit 'collides' with a finite amplitude periodic orbit thus forming an equilibrium-to-periodic heteroclinic connection. We consider only Hamiltonian reversible system of the lowest possible dimension to describe an unfolding of this scenario in a structurally stable way, namely 2 d.o.f. (4 dimensions of phase space). Although, this may seem restrictive, note that there is a so-called Homoclinic Center Manifold Theorem (Sandstede 1995), which loosely speaking states that four dimensions is enough to explain this phenomenon occuring in higher (even, in some circumstances, infinite) dimensional systems.

Therefore, consider a non-integrable, 2 d.o.f. Hamiltonian system with a saddle focus equilibrium O, which is in the fixed point set of a reversibility, whose unstable manifold contains a heteroclinic connection with a hyperbolic reversible periodic orbit L. Without loss of generality, suppose that both the equilibrium and the periodic orbit lie in $H(0)$, the zero level set of the Hamiltonian function. Furthermore, within $H(0)$, take a Poincaré section Π which contains O and is transverse to L. Note that this will not be a nondegenerate Poincaré section since it cannot be transverse to the flow near O; however this is unimportant, provided that Π is chosen to be transverse to the flow in the stable and

unstable manifolds of O. Then the intersections with Π of the stable and unstable manifolds of both O and L will all be one dimensional. Strictly speaking, in order to choose such a Poincaré section it is necessary to assume that these two manifolds do not intersect non-transversally, in which case we would have to argue more delicately. For the purposes of illustration though, we shall pretend that Π is globally defined even through homooclinic tangencies. Furthermore, choose Π such that it contains the portion within $H(0)$ of the fixed point set of the reversibility, the so-called symmetric section S. (See Fig. 3).

Our first observation from such a picture is that a heteroclinic connection between O and L persists under parametric perturbation. Hence, in order to consider a bifurcation phenomenon we have to consider a tangency between the unstable manifold of O, $W^u(O)$, and the stable manifold of L, $W^s(L)$.

Fig. 3 depicts the situation when $W^u(O)$ and $W^s(L)$ 'pass through' each other under parameter variation, including two successive heteroclinic tangencies (in panels (b) and (d)). Clearly the complete unfolding of this bifurcation would lead to a complex story involving periodic, homoclinic and heteroclinic orbits of various kinds. Here we focus only on the implications for the simplest homoclinic orbits to O, by which we mean orbits that spend a unique time interval outside a small neighbourhood of O. The existence of such homoclinic orbits can be inferred from points of intersection of $W^u(O) \cap \Pi$ and S, since, by reversibility, such points must be in the stable manifold of O also. This is illustrated in Fig. 3 by S acting like a mirror. Whenever the solid line $W^u(O)$ intersects S, its dashed mirror-image $W^s(O)$ intersects at the same point. The geometry of the heteroclinic tangle depicted in Fig. 3(c) (which can be rigourously established via the Lambda Lemma (Guckenheimer & Holmes 1983, Sect. 5.2) and the assumed sequence of heteroclinic tangencies) implies that for parameter values between those of the two tangencies, there will be an infinity of such intersection points. Moreover, information may be gleaned on the creation and destruction of the corresponding orbits, as is depicted in a bifurcation diagram in Fig. 4.

Fig. 4 shows that the infinity of simplest homoclinic orbits lie on a single wiggle curve. As the solution progresses up this curve it undergoes a succession of fold points which corresponding to points of tangency between $W^u(O)$ and S. In so doing, the homoclinic orbit gains an extra 'hump' by passing one more time in the neighbourhood of L. The wiggly curve accumulates on the parameter values of the two heteroclinic tangencies from the left in both cases, given the parameter dependence depicted. Hence viewing the bifurcation from left to right, the first tangency suddenly creates infinitely many homoclinic orbits, whereas the second one only starts the process of their destruction. Alternatively, viewing the bifurcation diagram from right to left, the overall effect of the bifurcation sequence is to remove a simple 'one-humped' homoclinic orbit, by repeatedly snaking back and forth in the bifurcation diagram, gaining more and more humps in the process, until it is indistinguishable from a O to L heteroclinic connection.

Finally in this section, note that the assumption of two successive heteroclinic tangencies is reasonable, since this would occur in small perturbations of completely integrable Hamiltonian systems containing a structurally unstable connection formed by the identification of $W^u(O)$ and $W^s(L)$. (See (Hirschberg & Laing 1995) for a similar assumption on successive *homoclinic* tangencies occuring in another context). Indeed, in work to be presented elsewhere (Woods & Champneys 1998), it will be shown that such a perturbation from an integrable heteroclinic connection occurs in an unfolding of the boundary between supercritical and subcritical Hamiltonian-Hopf bifurcation points.

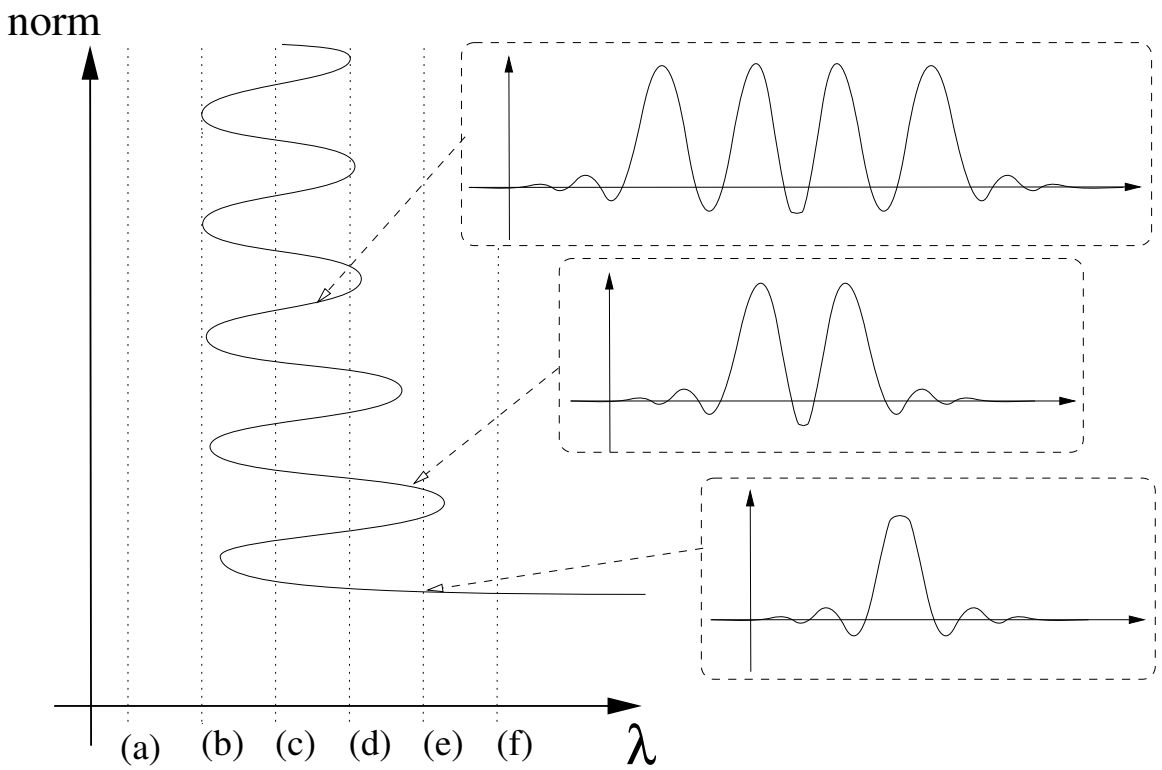

Figure 4: Bifurcation diagram of L^2-norm against bifurcation parameter λ of homoclinic solutions to O implied by the unfolding of successive heteroclinic tangencies between O and the periodic orbit L. Parameter values (a)-(f) refer to the corresponding panelss of Fig. 3.

5 Numerical Verification

5.1 Formulation

Numerical confirmation of the phenomena just outlined for the cylindrical shell requires careful formulation, taking care to compute the appropriate solutions among the infinite possibilities for a (theoretically infinitely) long cylinder. In our earlier work (Lord, Champneys & Hunt (1997, 1998)), an intensive examination of the homoclinic solutions was carried out by decomposing the circumferential component of the von Kármán–Donnell PDEs into M spectral modes via a Galerkin procedure, reducing them to $8M$ coupled nonlinear ODEs. There, we typically only computed localised buckling modes from their bifurcation point to the first minimum of load with respect to end shortening. Here we present results beyond this first minimum in order to illustrate their connection with the analysis of Sections 3 and 4, and in particular demonstate how this first minimum is linked to the existence of a heteroclinic connection.

We discretize the von Kármán–Donnell equations (1) and (2) in such a way as to exploit the natural symmetries in the problem. Experimentally a well defined number, s, of waves is observed circumferentially (Koiter 1945, Donnell & Wan 1950, Yamaki 1984) in the buckled deformation, corresponding to an invariance under rotation of $2\pi/s$. Hence we write

$$w(x,y) = \sum_{m=0}^{\infty} a_m(x)\cos(ms\rho y); \qquad \phi(x,y) = \sum_{m=0}^{\infty} b_m(x)\cos(ms\rho y), \qquad s \in \mathbb{N},$$

and refer to $\cos(s\rho y)$ as the *seed mode*. Substituting into the von Kármán–Donnell equations and taking the L^2 inner product with $\cos(ms\rho y)$ we obtain a system of non-linear ODEs for the Fourier modes a_m and b_m for $m = 0, \ldots, \infty$. The Galerkin approximation may then be formed by taking $m = 0, \ldots, M-1$ for some finite M giving a system of $8M$ first order ordinary differential equations. Note that $s = 1$ corresponds to the standard Galerkin (or Rayleigh-Ritz) approximation.

There is a further symmetry which plays an important role in localized buckling. Experimentally the observed patterns tend to be either *symmetric* or, more frequently, *cross-symmetric*. A solution to the von Kármán–Donnell equations that is symmetric about a section at $x = T$ satisfies

$$w(x, y) = w(2T - x, y) \qquad \& \qquad \phi(x, y) = \phi(2T - x, y), \tag{15}$$

whereas a solution which is cross-symmetric about a section at $x = T$ satisfies for some seed s

$$w(x, y) = w(2T - x, y + \pi R/s) \qquad \& \qquad \phi(x, y) = \phi(2T - x, y + \pi R/s). \tag{16}$$

It is not difficult to see that the symmetries defined by (15) and (16) imply a reversibility as described in Section 4. Thus we may define a fixed point sets, $\mathcal{S}$, of the reversibility forming $4M$-dimensional sub-manifolds of phase space $\mathbb{R}^{8M}$. We can then impose boundary conditions such that the solution we seek has $\mathcal{S}$ at its midpoint.

In fact, symmetric solutions are observed far less frequently in experiments than cross-symmetric solutions. Furthermore, when symmetric solutions do occur, they are generally for short cylinders and are less localized (cf (Yamaki 1984, Eßlinger 1970, Eßlinger & Geier 1972)). Note also that there is a degeneracy in the equations for the zero mode ($m = 0$) such that these may be solved for $a_0'', a_0''', b_0'', b_0'''$ independently of the initial conditions for a_0, a_0', b_0, b_0'. This corresponds to a trivial translational symmetry in the problem (sometimes called a rigid body mode).

The numerical method for computing the homoclinic orbits is described in detail in Lord, Champneys & Hunt (1998). We solve for (cross)-symmetric homoclinic solutions as a boundary value problem on a truncated domain with boundary conditions which at one end place the solution in the linearized unstable manifold of the trivial solution (see (Beyn 1990)) and at the other end exploit the boundary conditions from the section $\mathcal{S}$. To compute periodic solutions we again solve a boundary value problem with section $\mathcal{S}$ boundary conditions imposed at both ends.

In the computations below we have used a shell with the following properties:

$$R = 100\text{mm}, \qquad t = 0.247\text{mm}, \qquad \nu = 0.3, \qquad E = 5.56\text{GPa}, \tag{17}$$

which correspond to the experimental values taken by Yamaki (1984). For the sake of clarity we only describe the cross-symmetric case and concentrate on one particular seed mode: $s = 11$. Similar results hold in the symmetric case and with other seed modes.

Numerically we have found that it is convenient to take $M = 6$ as the best compromise between accuracy and efficiency. Qualitatively similar results have been obtained for smaller and larger M. Convergence as both M and the cylinder length are increased was discussed in Lord, Champneys & Hunt (1998); wider convergence questions are addressed in Lord, Peterhof, Sandstede & Scheel (1998).

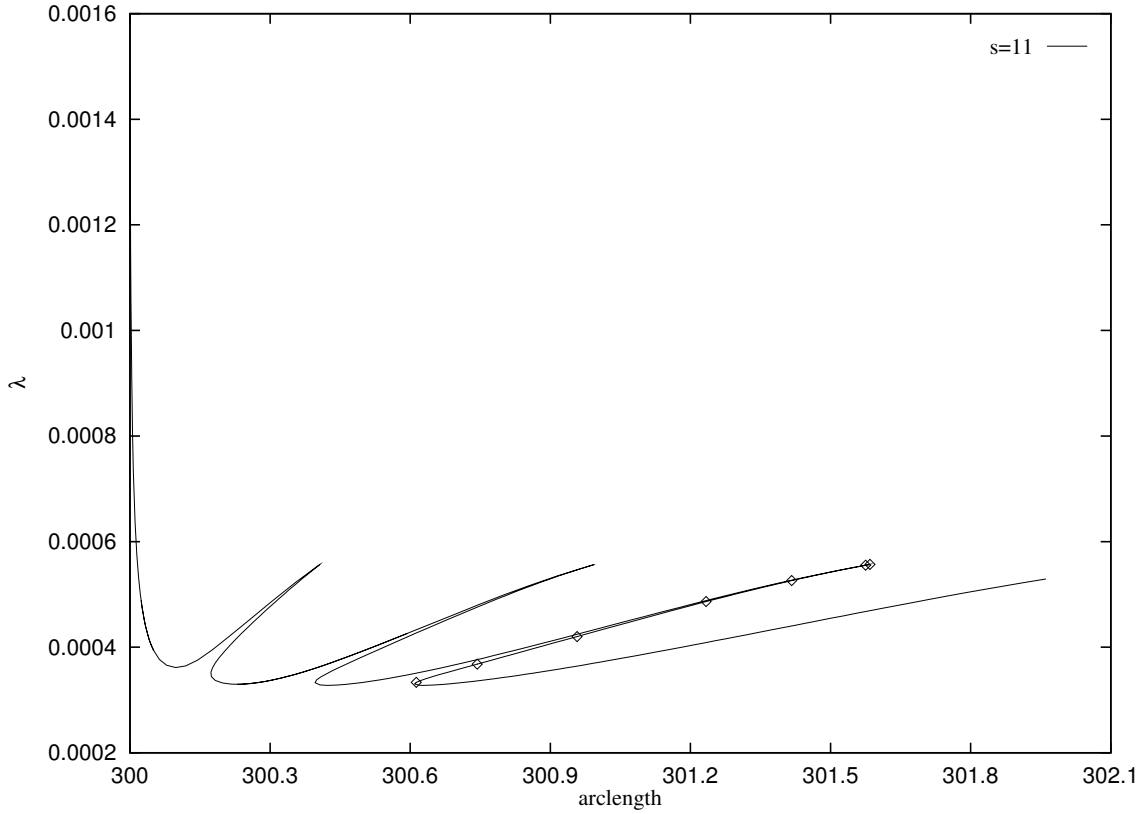

Figure 5: The localised buckling path plotting the loading parameter λ against the "arclength" measure of end shortening. Squares show the states plotted in Fig. 6. Diamonds indicate points at which the corresponding periodic orbit has been "chopped out" (see Fig. 7).

The equations are then solved in the continuation code AUTO (Doedel & Kernevez 1986), under parametric variation of the loading parameter $\lambda = P/Et$. The result from this is shown in Fig. 5 in the space of λ against a measure of the end-shortening given by the arclength of the solution computed to the section $\mathcal{S}$ at the line given by $y = 0$ on the cylinder:

$$\text{arclength} = \int_0^T \left[1 + \left(\sum_{k=0}^{M-1} \frac{\partial a_k}{\partial x} \right)^2 \right]^{1/2} \mathrm{d}x.$$

The fluctuating nature of the post-buckling curve signifies sequential localized buckling in qualitatively the same manner as in Fig. 4, as predicted by the dynamical system analysis. Fig. 6 presents several solutions to the equations along this path. For the initial post-buckling, a localization involves the single diamond pattern shown in Fig. 6(a). It restabilizes at the first minimum post-buckling load, whereupon under increasing load it then meets a second instability at a maximum limit point, signifying a second localized buckle concatenating with the first. This results in the addition of a further cell to the buckle pattern (Fig. 6(b)). The process continues to include any number of cells, three being shown in Fig. 6(c). One interpretation of this sequence of minima and maxima is thus that, starting from each minimum, we are essentially buckling an already deformed shell - each new buckle simply adds a new cell to the deformation. The limit of an infinite

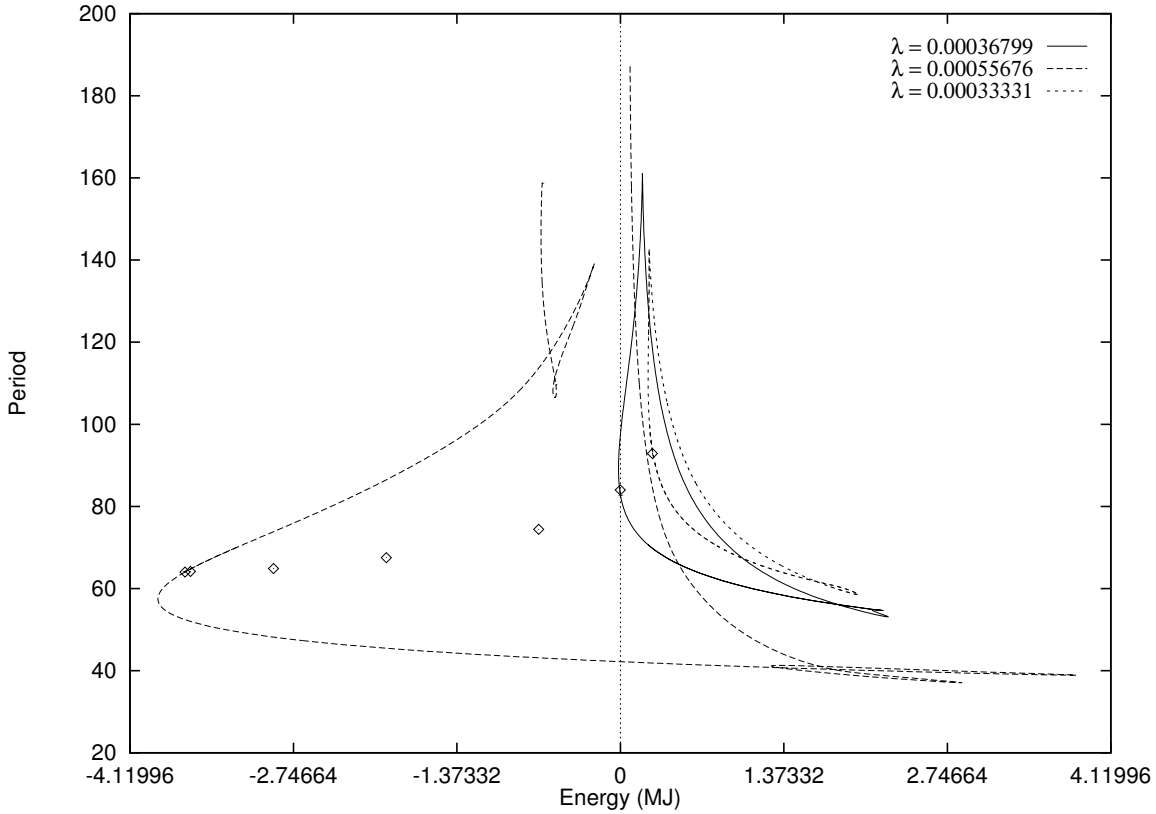

Figure 7: Curves of periodic solutions for $s = 11$ versus "scaled" potential energy ($\mathcal{V}$ of (6) divided by the period of the orbit). Also plotted as diamonds are the periodic orbits (obtained from the "chopped out" middle sections of the homoclinic orbits of Fig. 5) to which a heteroclinic connection occurs.

number of cells then represents heteroclinic connection from the flat state to periodic. It is therefore instructive to search for the periodic solution to which this connection occurs. Note that the homoclinic to periodic connection occurs over a range of loads (between the limiting values of the sequences of maxima and minuma along the buckling curve). To test the Maxwell load hypothesis, it would be interesting to see if there is some energetic critereon that picks out the periodic solution to which this connection is made, and to see how this relates to the first minimum on the branch of the localised buckling mode.

Periodic equilibrium states can be found from these buckled forms by "chopping out" the central section of the buckle pattern of Fig. 6(c) and forcing periodic boundary conditions. Although the chopped-out section is not precisely periodic, in our experience one step of continuation is usually enough to enforce it. Points at which the periodic solution is examined in this way are indicated by a diamond.

Different periodic states can arise depending on the boundary conditions; the full allowable range at any load level can be explored by continuation in the period while holding the load constant. Typical results at three different load levels are shown in Fig. 7 on a plot of period against "scaled" total energy (energy of equation (6), divided by period, to give energy per unit length). Periodic solutions in Fig. 7 marked by a diamond are those chopped from the homoclinic orbits of Fig. 5; of these, the smallest period (negative energy) solution corresponds to a maximum of the wiggle of Fig. 5, while the largest period (positive energy) solution corresponds to a minimum. To avoid clutter we have

plotted this curve at the three load values of $\lambda = 3.3331 \times 10^{-4}$, $\lambda = 5.5676 \times 10^{-4}$, and $\lambda = 3.6799 \times 10^{-4}$. We note that the last of these is close to, but just above, the first minimum load encountered on the post-buckling path, for which $\lambda = 3.6146 \times 10^{-4}$.

5.2 Comparisons

Interest naturally falls on the solution with minimum energy, at the leftmost point of each enclosed curve, as being that most likely to be linked with the localized solution that would arise in practice. In each of the curves we have computed, the periodic orbit associated with heteroclinic connection is at, or close to, this minimum energy solution.

We are particularly interested in the point at which the minimum energy is zero, predicted by the slow-space formulation as the Maxwell load below which no localized solution can occur. We see that the connection to the periodic with zero energy would occur at almost exactly the same value of the load as the first post-buckled minimum; the curve for $\lambda = 3.6799 \times 10^{-4}$ just crosses into the negative energy regime, so zero minimum energy would be found at a load just less than this value. Comparing values, we see that the first minimum occurs at $\lambda_M/\lambda_D = 0.242$ and the near-zero energy periodic solution at $\lambda_M/\lambda_D = 0.246$. Hunt & Lucena Neto (1993) give both the Maxwell load computed from periodic Rayleigh-Ritz analysis, and the minimum load reached experimentally, for $s = 11$ at $\lambda_M/\lambda_D = 0.24$. Thus the numerics suggest that the load at the first post-buckled minimum of a *localized* solution may be predicted from the energy of a *periodic* solution (given by the classical Maxwell load).

It is interesting also to compare aspect ratios β (ratio of axial to circumferential wavelengths) for the periodic solutions. The "chopped out" period of the near-zero energy curve of Fig. 7 gives $\beta = 1.47$. This compares favourably with the Maxwell load value of $\beta = 1.49$ for the Rayleigh-Ritz solution of Hunt & Lucena Neto (1993), and the best estimate of an experimental value of $\beta = 1.43$, taken from surface maps of the buckled cylinder found in Yamaki (1984).

6 Concluding Remarks

At this point it is a good idea to relate back to what might be observed in a realistic cylinder experiment. The form of load versus end-shortening diagram seen in Fig. 5 would not be expected in reality. In actual experiments under controlled end shortening (see for example Yamaki (1984) Fig. 3.52e, P. 231) the initially unbuckled shell destabilizes and undergoes a snap response into the buckled pattern at a load less than the classical bifurcation point; the stabilized buckling pattern that appears would typically be held at a load above the first minimum post-buckling load. Under further application of end-shortening the now-buckled shell would pass through the first minimum and start up towards the first maximum of Fig. 5. At some point along that curve the shell would lose stability and bifurcate typically into a mode in which the number of circumferential waves is reduced by one, equivalent to a change in the seed mode from s to $s-1$. In the work of Riks, Rankin & Brogan (1996) and Riks & Rankin (1996), a combination of statics and dynamics was used to attempt to form a numerical picture using finite elements of this phenomenon, allowing the shell to buckle dynamically to find the wave number s. In contrast, for simplicity we have fixed the subspace s in which we are working to examine the buckling phenomena, and used

these numerics to confirm predictions from the asymptotic analysis and dynamical systems analogy. Although the results presented here are for a single seed mode and for the cross-symmetric form of solution only, preliminary results indicate similar pictures for other seed modes and the symmetric case.

In particular we have shown that the concept of the Maxwell load obtained from the asymptotic approximation gives a good prediction of the first minimum post-buckling load. By considering the smallest allowable d.o.f. system that is capable of capturing the full dynamics, a more complete picture is obtained from the dynamic analogy. This demonstrates that an infinity of further minima lie between the first minimum and that of the periodic response, effectively bridging the gap between the localized and periodic responses of Fig. 2. The outcome is an oscillatory form of bifurcation diagram – between two well defined values with an associated heteroclinic tangle within the range – that must be seen as typical for systems that first destabilize and then restabilize. Our numerics confirm this form of behaviour in the von Kármán–Donnell equations.

References

Beyn, W.-J. (1990), 'The numerical computation of connecting orbits in dynamical systems', *IMA Journal of Numerical Analysis* **9**, 379–405.

Buffoni, B., Champneys, A. R. & Toland, J. F. (1996), 'Bifurcation and coalescence of a plethora of homoclinic orbits for a Hamiltonian system', *J. Dyn. Diff. Eq.* **8**, 221–281.

Champneys, A. R. (1998), 'Homoclinic orbits in reversible systems and their applications in mechanics, fluids and optics', *Physica D* **112**, 158–186.

Champneys, A. R., Hunt, G. W. & Thompson, J. M. T., eds (1997), *Localisation and solitary waves in solid mechanics.* Special Issue of *Phil. Trans. Roy. Soc. Lond. A.* **355** 2073-2213.

Devaney, R. (1976), 'Reversible diffeomorphisms and flows', *Trans. Amer. Math. Soc.* **218**, 89–113.

Doedel, E. & Kernevez, J. P. (1986), AUTO: Software for continuation problems in ordinary differential equations with applications, Technical report, California Institute of Technology. Applied Mathematics Technical Report.

Donnell, L. H. & Wan, C. C. (1950), 'Effect of imperfections on buckling of thin cylinders and columns under axial compression', *J. of Applied Mechanics* **APM-14**(49), 73–83.

Eßlinger, M. (1970), 'Hochgeschwindigkeitsaufnahmen vom beulvorgang dünnwandiger, axialbelasteter zylinder', *Der Stahlbau.*

Eßlinger, M. & Geier, B. (1972), 'Gerechnete nachbeullasten als untere grenze der experimentallen axialen beullasten von kreiszylindern', *Der Stahlbau.*

Golubitsky, M. & Schaeffer, D. (1985), *Singularities and groups in bifurcation theory, Vol. 1*, Applied Mathematical Sciences; 51, Springer-Verlag, Berlin.

Guckenheimer, J. & Holmes, P. (1983), *Nonlinear Oscillations, Dynamical Systems and Bifurcations of Vector Fields*, Applied Mathematical Sciences, 42, Springer-Verlag, New York, U.S.A.

Hirschberg, P. & Laing, C. (1995), 'Sucessive homoclinic tangencies to a limit cycle', *Physica D* **89**, 1–14.

Hunt, G. W. & Lucena Neto, E. (1991), 'Localized buckling in long axially–loaded cylindrical shells', *J. Mech. Phys. Solids* **39**(7), 881–894.

Hunt, G. W. & Lucena Neto, E. (1993), 'Maxwell critical loads for axially-loaded cylindrical shells', *ASME J. Appl. Mech.* **60**(3), 702–706.

Hunt, G. W. & Wadee, M. K. (1991), 'Comparative Lagrangian formulations for localised buckling', *Proc. R. Soc. Lond. A* **434**, 485–502.

Hunt, G. W., Bolt, H. M. & Thompson, J. M. T. (1989), 'Structural localisation phenomena and the dynamical phase-space analogy', *Proc. R. Soc. Lond. A* **425**, 245–267.

Iooss, G. & Peroueme, M. C. (1993), 'Perturbed homoclinic solutions in reversible 1:1 resonance vector fields', *J. Diff. Eq.* **102**, 62–88.

Koiter, W. T. (1945), On the Stability of Elastic Equilibrium, PhD thesis, University of Delft. English Translation: Tech. Rep. AFFDL-TR-70-25 Air Force Flight Dyn. Lab. 1970.

Lord, G. J., Champneys, A. R. & Hunt, G. W. (1997), 'Computation of localized post buckling in long axially–compressed cylindrical shells', *Phil. Trans. Roy. Soc. Lond. A* **355**, 2137–2150. in Theme Issue on *Localization and Solitary Waves in Solid Mechanics*.

Lord, G. J., Champneys, A. R. & Hunt, G. W. (1998), 'Computation of homoclinic orbits in partial differential equations: an application to cylindrical shell buckling'. To appear in *SIAM J. Sci. Comp.*

Lord, G. J., Peterhof, D., Sandstede, B. & Scheel, A. (1998), 'Numerical computaton of solitary waves in semilinear elliptic problems on infinite cylinders'. To be submitted.

Mielke, A. (1991), *Hamiltonian and Lagrangian flows on center manifolds: with applications to elliptic variational problems*, Lecture notes in mathematics; 1489, Springer-Verlag, Berlin.

Potier-Ferry, M. (1983), Amplitude modulation, phase modulation and localisation of buckle patters, *in* J. M. T. Thompson & G. W. Hunt, eds, 'COLLAPSE: the buckling of structures in theory and practice', Cambridge University Press.

Riks, E. & Rankin, C. C. (1996), Computer simulation of the buckling behavior of thin shells under quasi static loads, *in* M. Kleiber, E. Onate & O. Zienkiewicz, eds, 'Computer Methods in Applied Mechanics', CAM. To Appear.

Riks, E., Rankin, C. C. & Brogan, F. A. (1996), 'On the solution of mode jumping phenomena in thin-walled shell structures', *Computer methods in applied mechanics and engineering* **136**(1), 59–92.

Sandstede, B. (1995), Center manifolds for homoclinic solutions, Technical report, Weierstraß Institut für Angewandte Analysis und Stochastik. Preprint No. 186.

Sandstede, B. (1997), 'Instability of localised buckling modes in a one-dimensional strut model', *Philosophical Transactions of the Royal Society of London, A* **355**, 2083–2097.

Thompson, J. M. T. & Hunt, G. W. (1973), *A general theory of elastic instability*, Wiley, London.

Tvergaard, V. & Needleman, A. (1980), 'On the localisation of buckle patterns', *ASME J. Appl. Mech.* **47**, 613–619.

van der Meer, J. (1985), *The Hamiltonian Hopf bifurcation*, Lecture notes in mathematics, 1160, Springer-Verlag, Berlin.

Woods, P. D. & Champneys, A. R. (1998), 'Heteroclinic tangles in the unfolding of a degnerate Hamiltonian Hopf bifurcation'. In preparation.

Yamaki, N. (1984), *Elastic Stability of Circular Cylindrical Shells*, Vol. 27 of *Applied Mathematics and Mechanics*, Elsevier.

Zeeman, E. (1977), *Catastrophe Theory: Selected Papers 1972–1977*, Addison-Wesley, London.